

A CRITICAL REVIEW ON WIRELESS POWER TRANSFER SYSTEMS USING METAMATERIALS

Pham Thanh Son¹, Bui Xuan Khuyen¹, Bui Son Tung¹, Le Thi Hong Hiep^{2,3},
Vu Dinh Lam^{2,*}

¹*Institute of Materials Science, Vietnam Academy of Science and Technology,
18 Hoang Quoc Viet, Cau Giay, Ha Noi, Viet Nam*

²*Graduate University of Science and Technology, Vietnam Academy of Science and Technology,
18 Hoang Quoc Viet, Cau Giay, Ha Noi, Viet Nam*

³*Fundamental of Fire Engineering Faculty, University of Fire Prevention and Fighting,
243 Khat Duy Tien, Thanh Xuan, Ha Noi, Viet Nam*

*Emails: lamvd@gust-edu.vast.vn

Received: 25 February 2022; Accepted for publication: 16 April 2022

Abstract. Recently, wireless power transfer (WPT) has been a topic of interest due to its attractive applications in modern life. Starting from Tesla's idea about a century ago, WPT has developed tremendously and appeared in many of the most modern electronic devices. However, some WPT systems still have limitations such as short transmission distance, low transfer efficiency, and electromagnetic leakage. Magnetic metamaterial (MM) is a potential candidate that can overcome the above disadvantages of WPT. This paper is intended to present an overview of recent advances and research progress on WPT systems. Three classes of WPT consisting of short-range, mid-range, and long-range, will be analyzed in detail both in terms of fundamentals and applications. Especially, MM configurations can be used to enhance the near-field WPT efficiency and reduce the leakage of electromagnetic field will also be evaluated. This article is expected to provide a comprehensive review of the mechanism and applications as well as the future development of metamaterial-based WPT systems.

Keywords: Wireless power transfers, metamaterials, negative permeability, evanescent wave.

Classification numbers: 2.1.2, 2.2.1, 4.1.

1. INTRODUCTION

Nowadays, mobile devices and especially wearable devices are an indispensable part of modern life. The market for such devices is therefore also growing rapidly with more and more intelligent, compact, and convenient products. Integrated circuit technology has evolved continuously over the years. Since then, new features are constantly being added to these devices along with faster processors. More tasks need to be processed, which in turn requires more power. Many energy storage solutions to supply mobile devices have been deployed, such as supercapacitors, lithium-ion batteries, solar cells, etc. However, storage technology on mobile

devices has not made significant improvements over the years. Therefore, powering or charging these devices is a matter of concern [1 - 3]. Wireless power transfer (WPT) was introduced more than a century ago by genius scientist Nikola Tesla with his invention for both types of WPT using radiated field (far-field) and induced field (near-field) [4]. WPT has been used to power implantable devices since the 1970s. Studies on the use of microwave energy to power aircraft have also been conducted since the 1960s [5 - 6]. However, this technology only really exploded in the era of mobile devices. The most popular wireless charging standard today is Qi, which has appeared in many of the most modern smartphones and smartwatches [7 - 11].

WPT technology can be implemented in three main directions: WPT is based on magnetic induction at close distance (mm-cm) [12 - 14], WPT is based on magnetic resonance at medium distance (cm-m) [15], and WPT is based on the radiated field at long distance (m-km) [16, 17]. Depending on the transmission distance and power required, a WPT type will be selected. In daily life applications, such as charging for smartphones, electric vehicles, and appliances WPT based on near-field is more commonly used [18 - 20]. WPT has also found many applications in biomedical implant devices [21 - 23].

Researchers have recently focused on magnetic resonance WPT because of the advantage of transfer distance and high efficiency [24, 25]. The magnetic resonance WPT can be explained using coupled-mode theory [26-28]. When the transfer distance increases, the coupling between resonators is reduced, which results in an efficiency drop [29]. Many studies reported that metamaterials with the ability to amplify evanescent waves could be utilized to improve the WPT system's performance [30-34].

This paper aims to conduct a comprehensive investigation of modern trends in WPT and the advantage of metamaterials in near-field WPT. The rest of this paper is organized as follows. Section 2 introduces the fundamentals of WPT for both far-field and near-field. The principle of metamaterials for the WPT system is presented in Section 3. Three main types of metamaterial-based WPT for efficiency improvement, misalignment compensation, and leakage field reduction are investigated in Section 4. Section 5 discusses the perspective and challenges of metamaterial-based WPT systems. Finally, the conclusion will be remarked in Section 6.

2. FUNDAMENTAL OF WPT: FROM FAR-FIELD TO NEAR-FIELD

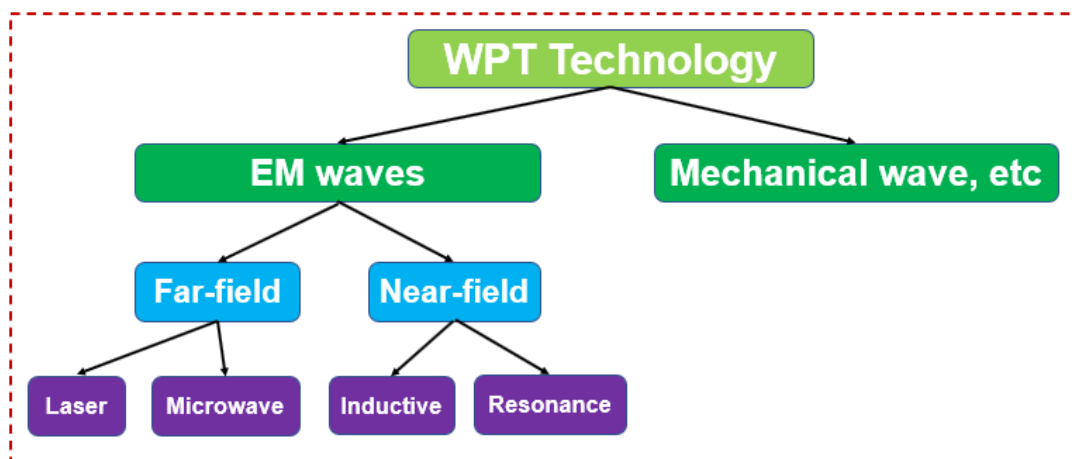


Figure 1. WPT technology classification.

In general, the category of the WPT technology under study is illustrated in Fig. 1 [35]. WPT means using waves rather than wires to transmit energy. Several kinds of waves can be utilized, but the most common is electromagnetic (EM) waves. Far-field WPT is for long-distance, while near-field WPT is widely used in daily applications [36 - 37].

2.1. Far-field WPT system

Over a long-distance, energy is transferred from a transmitting antenna to a receiving antenna through electromagnetic waves. Such WPT system has advanced in long-distance transmission, suitable for information transfer. However, it can affect the human body due to electromagnetic radiation. Thus, WPT systems must be carefully designed [38 - 39]. In 1963, W. C. Brown first demonstrated the far-field WPT in the microwave range at 2.45 GHz [17]. Radiative energy can be departed from an antenna and travels through the air over a long distance in the form of electromagnetic waves. However, the power transfer efficiency was low due to high power loss [3].

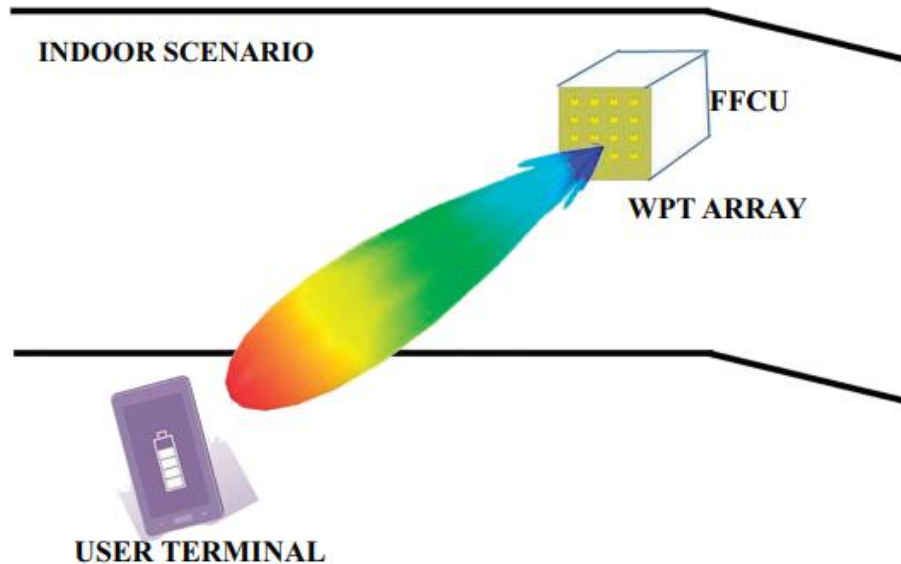


Figure 2. Antenna array for the far-field charging unit in wireless power transfer [40].

2.2. Near-field WPT system

Far-field WPT is applicable for various applications where efficiency is not a concern, and the entire system could be illuminated with microwave radiation without exceeding safety standards [41]. However, for high efficiency and daily life, near-field WPT is more suitable [42]. It is possible to use both electric and magnetic fields for near-field power transmission [43]. The near-field magnetic solution will allow transmission through various obstacles and people since the magnetic field will not interact with them while the electric field causes polarization. Therefore, most of WPT's commercial products are based on magnetic near-field WPT [44 - 46].

2.2.1. Short-range near-field WPT system (Inductive coupling WPT)

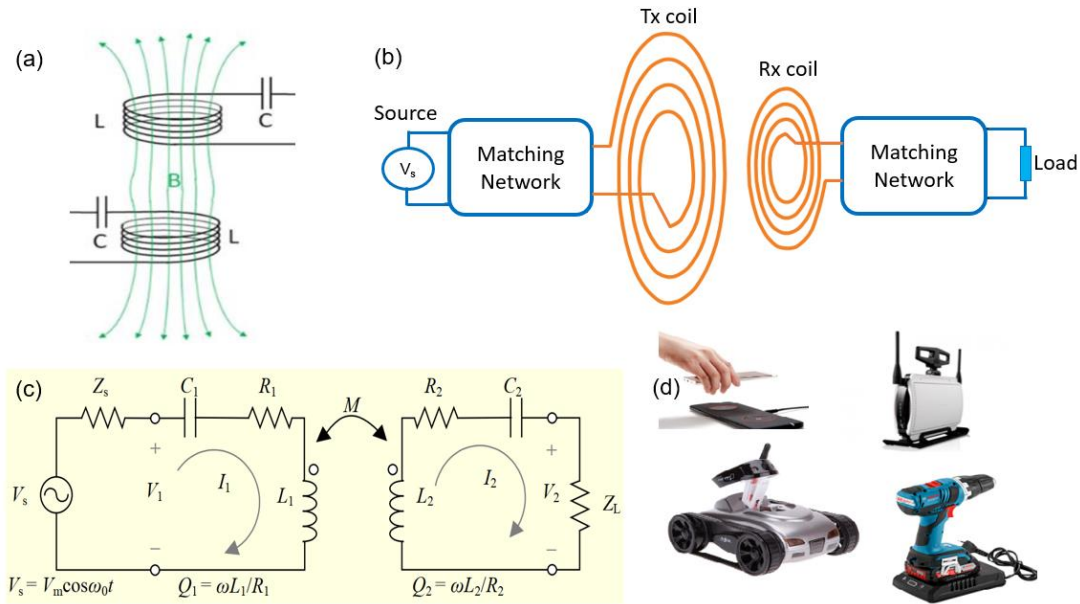


Figure 3. Inductive coupling WPT. (a) 2-coil system [12], (b) schematic, (c) circuit model [47], (d) applications [48].

The magnetic inductive coupling WPT mechanism is indicated in Fig. 3(a). The system consists of two coils (transmitter and receiver coils) placed close together. An alternating current at a high frequency is excited to the transmitter coil, generating an oscillating magnetic field by Ampere’s law. The magnetic field passes through the receiving coil and induces an alternating current in the receiver coil. That is how energy transfers from transmitter to receiver. The schematic of the 2-coil WPT system is shown in Fig. 3(b). To make the energy transfer process more efficient, two matching networks are embedded between source-transmitter coils and load-receiver coils. Figure 3(c) shows the equivalent circuit model of a 2-coil WPT system with voltage applied V_s , source, and load impedance R_s and R_l . The self-inductance and self-capacitance of the coils are depicted by L_T , L_R , C_T , and C_R , respectively. Because the 2-coil WPT system operates in the low MHz frequency range, the radiation loss of the coil can be ignored. Therefore, the intrinsic loss of the coils is mainly caused by Ohmic loss, denoted by R_T and R_R . As we know, there is a current I_i flowing in the coils due to inductive coupling between the two coils. Two coils are coupled to each other through the mutual inductance M , given by $M = k\sqrt{L_T L_R}$, where k is the coupling coefficient. Nowadays, 2-coil WPT systems are very popular in modern electronic devices, such as wireless chargers for smartphones, power drills, and self-propelled equipment, as shown in Fig. 3(d).

To quantify the energy transfer efficiency, we analyze the equivalent circuit model of the WPT system. First, we consider the behavior of an isolated resonator. It can be described by two essential parameters: self-resonant frequency $\omega_0 = 1/\sqrt{LC}$ and intrinsic loss factor Γ . The relationship between these two parameters defines the quality factor (Q -factor) of the resonator coil, which can be expressed as follows:

$$Q = \frac{\omega_0}{2\Gamma} = \omega_0 \frac{L}{R} \quad (1)$$

The expression for Q -factor in Eq. (1) shows that reducing the loss in the circuit (R) leads to an increase in the Q -factor. Q -factor is a parameter to measure how well the resonator stores energy, and the WPT system needs a high Q -factor for more efficient energy transfer.

Analyzing the circuit in Fig. 3(c), we obtain the ratio of power delivered to the load resistor and supply power available from the source at the resonant frequency.

$$\frac{P_L}{P_S} = \frac{4 \cdot k^2 Q_T Q_R \frac{R_S}{R_T} \frac{R_L}{R_R}}{\left[\left(1 + \frac{R_S}{R_T} \right) \left(1 + \frac{R_L}{R_R} \right) + k^2 Q_T Q_R \right]^2} \quad (2)$$

From Eq. (2), we can get the best system performance if we have:

$$\frac{R_S}{R_T} = \frac{R_L}{R_R} = \sqrt{1 + k^2 Q_T Q_R} \quad (3)$$

Then the optimum efficiency of the WPT system can be given by:

$$\eta_{opt} = \frac{k^2 Q_T Q_R}{\left(1 + \sqrt{1 + k^2 Q_T Q_R} \right)^2} \quad (4)$$

In a symmetric system, the transmitter and receiver coils are identical, so $Q = Q_T = Q_R$. Therefore, Eq. (4) can be simplified as follows:

$$\eta_{opt} = \frac{k^2 Q^2}{\left(1 + \sqrt{1 + k^2 Q^2} \right)^2} \quad (5)$$

As can be inferred from Eq. (5), the kQ product is an essential coefficient of the inductive coupling WPT system. While Q is dependent on the shape and material of the coil, k is presented for the distance between transmitter and receiver of the WPT system or the so-called efficiency transfer distance.

2.2.2. Mid-range near-field WPT system (Magnetic resonant coupling WPT)

The inductive coupling WPT offers a variety of solutions for contactless charging systems. However, the short transfer distance has limited the range of its applications. Therefore, many researchers have worked to extend the transfer distance of near-field WPT systems [51-56]. Kurs *et al.* [26] at Massachusetts Institute of Technology (MIT) proposed an approach with four coils, utilizing two resonator structures at the same resonant frequency to enhance the efficiency of WPT system. This is called magnetic resonant WPT (MR-WPT) system or 4-coil WPT system. Figure 4(a) shows the experiment setup of Zhang *et al.* for transferring energy through the air with a distance of 2.5 m to light two 60 W bulbs. Figure 4(b) illustrates a schematic of a MR-WPT system using two coupled resonators, which consists of 4 coils: source coil, transmitter resonator (Tx), receiver resonator (Rx), and load coil. The distances between source coil – Tx and load coil – Rx are small so that they can interact with each other via inductive coupling. The gap between Tx and Rx defines the efficiency transfer distance of the MR-WPT system. Tx and Rx have the structure with multi-turn of cooper. Therefore, they have a high Q -factor (400 in [57

- 58]) to transfer energy efficiently. As discussed in the previous section, the transfer efficiency of a WPT system strongly depends on kQ product. In the MR-WPT system, the Q -factor is very high, even if the coupling is very small, the transfer efficiency can still be achieved at a good value, which means the transfer distance can be extended. The MR-WPT system can be represented by an equivalent circuit, as shown in Fig. 4(c). In the transmitter part, the source loop is excited by a voltage V_S with the output impedance R_S . The source loop can be modeled as an inductor (L_1), capacitor (C_1), and resistor (R_1). The Tx consists of a multi-turn air-core spiral inductor (L_2), capacitor (C_2), and resistor (R_2). Two inductors L_1 and L_2 are connected with coupling coefficient k_{12} . The receiver part is defined similarly and linked with the transmitter part by coupling coefficient k_{23} . In a typical implementation of the MR-WPT system, the distance between the source loop and Tx would be fixed so that k_{12} is constant.

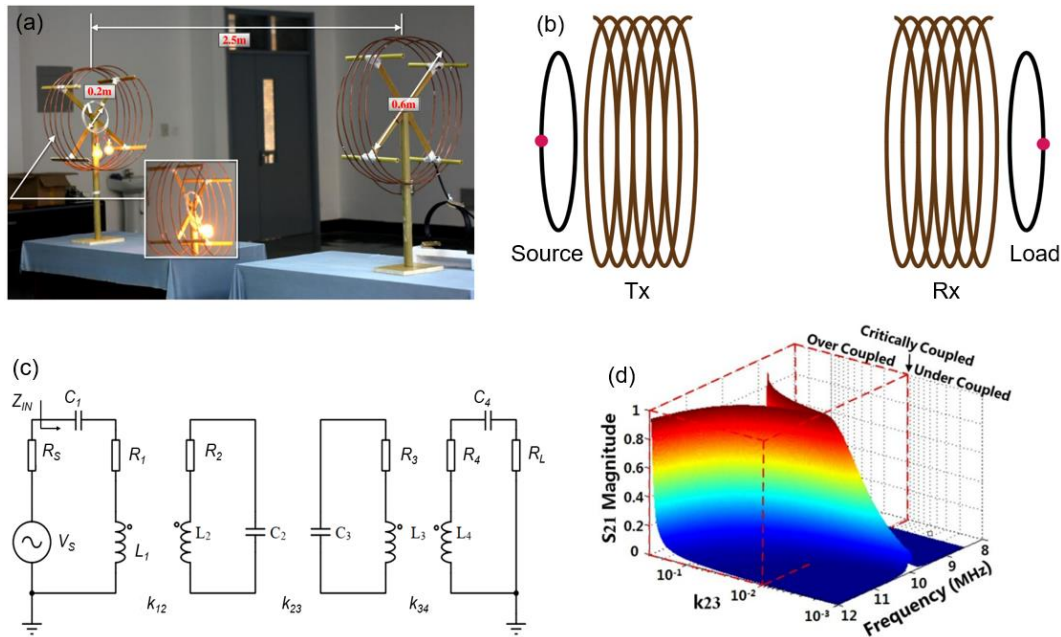


Figure 4. Magnetic resonant WPT. (a) WPT via 2.5 m distance [49], (b) schematic of 4-coil system [2]. Copyright 2017 AIP Publishing LLC. (c) Circuit model [50], (d) Efficiency of MR-WPT system [15].

Similarly, k_{34} would also be fixed. Therefore, the distance between transmitter and receiver results in k_{23} which is the remaining uncontrolled value.

To analyze the circuit in Fig. 4(c), we apply Kirchhoff's voltage law (KVL) to determine the current in each resonant circuit:

$$\begin{cases} V_S = \left(R_S + R_1 + j\omega L_1 + \frac{1}{j\omega C_1} \right) I_1 + j\omega M_{12} I_2 \\ 0 = \left(R_2 + j\omega L_2 + \frac{1}{j\omega C_2} \right) I_2 + j\omega M_{12} I_1 + j\omega M_{23} I_3 \\ 0 = \left(R_3 + j\omega L_3 + \frac{1}{j\omega C_3} \right) I_3 + j\omega M_{23} I_2 + j\omega M_{34} I_4 \\ 0 = \left(R_L + R_4 + j\omega L_4 + \frac{1}{j\omega C_4} \right) I_4 + j\omega M_{34} I_3 \end{cases} \quad (6)$$

where: I_i ($i = 1-4$) is the current in coils, $M_{ij} = k_{ij}\sqrt{L_i L_j}$ denotes mutual coupling between coils, ω is the angular operating frequency of the WPT system.

When the MR-WPT is symmetric, the source/load coils are identical, and so are the Tx/Rx coils. We obtain $Q_1 = Q_4$; $Q_2 = Q_3$ và $k_{12} = k_{34}$. The voltage ratio between the load and the source which is an essential quantity for the performance of the WPT system can be calculated by the following formula:

$$\left| \frac{V_L}{V_S} \right| = \left| \frac{I_4 R_L}{I_1 R_S} \right| = \frac{k_{23} k_{12}^2 Q_1 Q_2^2}{(1 + k_{12}^2 Q_1 Q_2)^2 + k_{23}^2 Q_2^2} \sqrt{\frac{R_L}{R_S}} \quad (7)$$

The transfer efficiency η is defined as:

$$\eta = \frac{P_{OUT}}{P_{IN}} = \frac{V_L^2 / R_L}{V_S^2 / 4R_S} = |S_{21}|^2 \quad (8)$$

where P_{OUT} and P_{IN} are output and input power, S_{21} is the transmission coefficient of the MR-WPT system.

An MR-WPT system operates in two modes, over-coupling and under-coupling, as shown in Fig. 4(d). When the coupling between Tx and Rx exceeds a critical value, the MR-WPT system operates at over-coupling regime; otherwise, it works at under-coupling regime. At over-coupling regime, frequency splitting is clearly visible at a distance shorter than the critical point. As the distance between Tx and Rx increases, the frequency separation decreases until the two modes converge at the critical point.

3. MAGNETIC METAMATERIAL APPLY IN WPT

Artificially engineered composites, the so-called metamaterials, have exotic electromagnetic characteristics that conventional materials do not show. Victor Veselago first proposed the concept of metamaterials in 1968 by a theoretical analysis of substances with negative permittivity (ϵ) and permeability (μ) simultaneously [59]. After 30 years of waiting, the first practical realization of metamaterial was made possible by two papers that presented negative epsilon using wire structure and negative permeability using split ring medium of John Pendry in 1996 and 1999, respectively [60 - 61]. Metamaterials present many novel phenomena which are not observed in natural materials, such as evanescent wave amplification [62], backward wave propagation, inverse Doppler effect, negative Goos-Hanchen shift, and backward Cerenkov radiation [63 - 66]. From their various unique properties, metamaterials can find many applications in the fields of energy harvesting [67], perfect absorber [68 - 72], enhancing antenna efficiency [73], and biosensors [74].

Depending on the signs of ϵ and μ values, the materials are classified into four groups: double-positive, epsilon-negative, double-negative, and mu-negative materials. In mu-negative material, only magnetic component is considered; therefore, it is also known as magnetic metamaterial (MM). Almost metamaterial structures operate at GHz and THz frequency range with both electric and magnetic responses [75, 76]. However, MM usually operates at low megahertz frequency and works mainly with magnetic field [77]. Thanks to negative permeability properties, MM can enhance the evanescent wave in the near-field region. Therefore, they can improve the WPT efficiency [78].

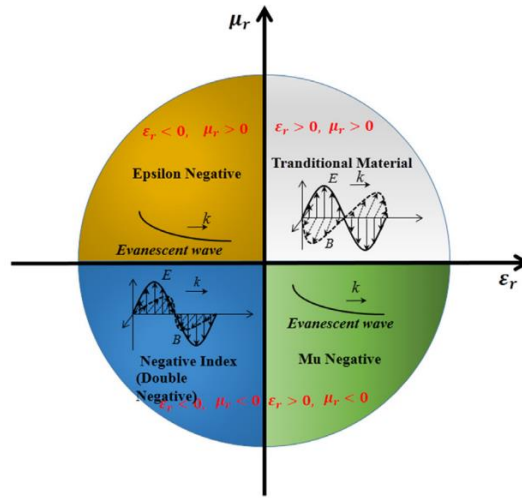


Figure 5. The categorization of materials based on permittivity (ϵ) and permeability (μ) [35].

3.1. Effective medium theory

Electromagnetic parameters representing the characteristics of metamaterials, such as permittivity (ϵ) and permeability (μ) can be achieved from the effective medium theory. When the unit cell of the material structure is much smaller than the operating wavelength of the electromagnetic wave, the material can be considered similar to a homogeneous medium. Therefore, the electromagnetic parameters of the material can be calculated using the effective medium theory. Ordinarily, the size of the metamaterial unit cell is less than $\lambda/50$, where λ is the operation wavelength. The effective permittivity and permeability of the metamaterial structure can be achieved by the S -parameter retrieval method, which was proposed in [79, 80]. From 1970, the Nicolson-Ross-Weir method [81] was usually used to calculate material parameters via transmission and reflection coefficients. On that basis, in 2004, X. D. Chen's research group [82] proposed a more accurate method to calculate the effective parameters of metamaterials.

The relationship of S -parameters and refractive index (n) and impedance (z) can be expressed as:

$$S_{11} = \frac{R_{01}(1 - e^{i2nk_0d})}{1 - R_{01}^2 e^{i2nk_0d}} \quad (9)$$

$$S_{21} = \frac{(1 - R_{01}^2)e^{ink_0d}}{1 - R_{01}^2 e^{i2nk_0d}} \quad (10)$$

where $R_{01} = (z-1)/(z+1)$, and $X = 1/2S_{21}(1 - S_{11}^2 + S_{21}^2)$, we have $e^{ink_0d} = X \pm i\sqrt{1 - X^2}$.

The refractive index n and wave impedance z can be expressed as:

$$n = \frac{1}{k_0d} \left\{ \left[\left[\ln(e^{ink_0d}) \right]^r + 2m\pi \right] - i \left[\ln(e^{ink_0d}) \right]^i \right\} \quad (11)$$

$$z = \pm \sqrt{\frac{(1 + S_{11})^2 - S_{21}^2}{(1 - S_{11})^2 - S_{21}^2}} \quad (12)$$

The effective permittivity and permeability can be calculated from the refractive index and wave impedance by:

$$\epsilon_{eff} = \frac{n}{z}; \quad (13)$$

$$\mu_{eff} = nz$$

Generally, the above approach is useful for calculating the effective permittivity and permeability of metamaterial structure. However, this approach is not convenient for obtaining effective permeability for the magnetic metamaterial working mainly in the near-field region.

According to the Lorentzian-type resonance, the effective permeability can be achieved by the following equation [61, 79]:

$$\mu_{eff} = F \left(\omega_0^2 - \omega^2 - \frac{j\omega\omega_0}{Q} \right); \quad (14)$$

$$Q = \frac{\omega L}{R} = \frac{\sqrt{L/C}}{R}; \quad (15)$$

$$F = \frac{\mu_0 A}{VL_{avg}}; \quad (16)$$

where F is the fill factor and Q is the quality factor of the unit cell, respectively. ω and ω_0 are angular frequency and angular resonance frequency of the unit cell, respectively. μ_0 is the permeability of the vacuum. A represents the area of the pattern of unit cell. V stands for the occupied volume unit cell. L_{avg} is the average inductance.

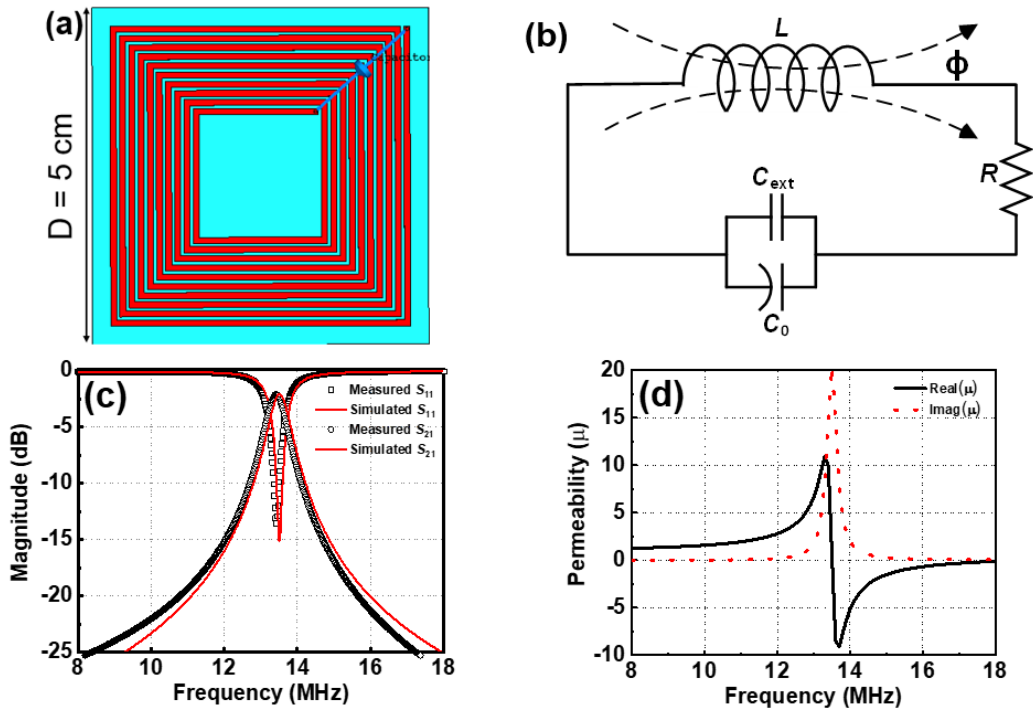


Figure 7. (a) Magnetic metamaterial unit cell, (b) schematic of unit cell, (c) reflection and transmission response, (d) permeability [83].

Figure 7(a) illustrates a diagram of MM unit cell consisting of a multi-turn spiral resonator loaded with a lumped capacitor. The equivalent circuit model of MM unit cell is shown in Fig. 7(b) with self-inductance $L = 0.95 \mu\text{H}$, self-capacitance $C_0 = 5.05 \text{ pF}$, the external capacitor has the value of $C_{\text{ext}} = 15 \text{ pF}$, R represents the ohmic losses in the spiral.

The resonant frequency of the MM unit cell can be calculated by:

$$f = \frac{1}{2\pi\sqrt{L(C_0 + C_{\text{ext}})}} \quad (17)$$

The reflection and transmission response of MM unit cell are shown in Fig. 7(c). A dip in the magnitude of S_{11} appears at 13.56 MHz, which is the resonant frequency of MM unit cell. The real and imaginary parts of permeability can be achieved from S-parameter by the standard retrieval method [84] and which is shown in Fig. 7(d). The real part of permeability has a narrow negative band around 13.56 MHz and the most significant negative permeability value of -9.5 at 13.68 MHz.

3.2. Evanescent wave amplification

The negative permeability metamaterial prohibits propagating waves, but they can amplify evanescent waves in the subwavelength regime [85, 86]. A WPT system uses magneto-quasistatic waves whose wavelength is much larger than the total size of the system. Therefore, the evanescent wave amplification property of magnetic metamaterials can be applied to enhance the efficiency of the WPT system.

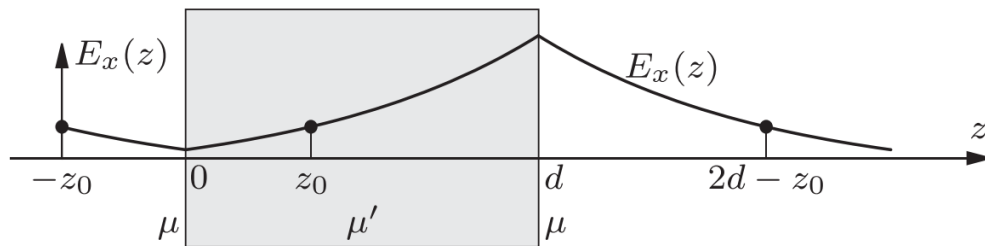


Figure 7. The evanescent wave is amplified through the negative permeability metamaterial [85]. Copyright 2017 AIP Publishing LLC.

Figure 7 describes the evanescent wave amplification in the negative permeability metamaterial. The negative permeability falls from 0 to d on the z -axis. The transmission and reflection coefficients at the matching boundary conditions of $z = 0$ and $z = d$ can be calculated by [85]:

$$T = \frac{(1 - r^2) e^{-2jk_z d}}{1 - r^2 e^{-2jk_z d}}; \quad (18)$$

$$r = \frac{\Psi - 1}{\Psi + 1}; \quad (19)$$

$$\Psi_{TM} = \frac{k_z \mu'}{k_z \mu}; \quad (20)$$

$$\Psi_{TE} = \frac{k'_z \varepsilon}{k_z \varepsilon}; \quad (21)$$

where $k'_z = \pm \sqrt{\omega^2 \mu \varepsilon - k_x^2}$, k_x represents x -component of incident wavenumber in free space, μ' is the permeability of metamaterial medium. When $\mu' = -1$ we obtain $T = e^{jk_z d}$.

Normally, in the free space, the amplitude of the evanescent wave decreases as the transfer distance increases. Nevertheless, the evanescent wave is amplified when the incident wave meets the negative permeability metamaterial medium.

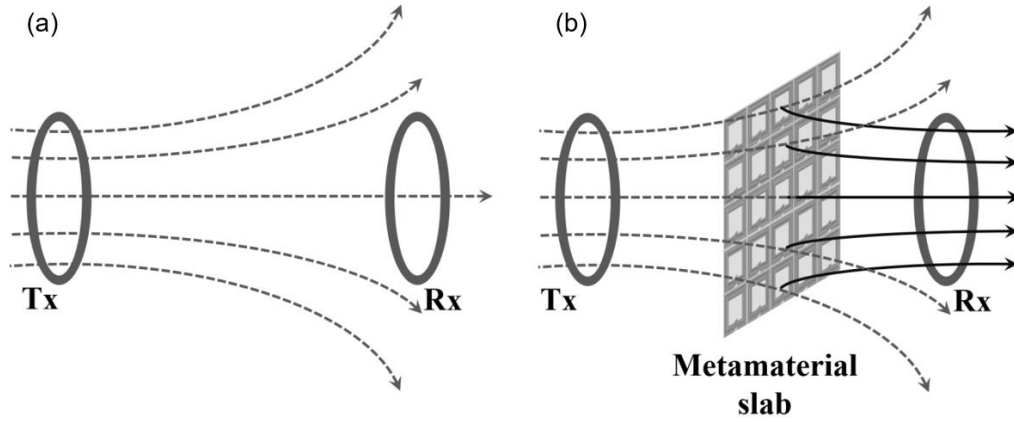


Figure 8. Improving the WPT efficiency by metamaterial slab: (a) WPT system in the free space, (b) WPT system with a metamaterial slab [87]. Copyright 2020 Cambridge University Press.

Figure 8 shows a schematic explanation for the principle of improving WPT efficiency using magnetic metamaterial. Figure 8(a) illustrates a basic WPT system with Tx and Rx coils. The magnetic field is generated by Tx coil shows its flux lines symmetrically around the center-center coils line. One problem is that Rx cannot capture all the magnetic flux produced by Tx. Therefore, the performance of this WPT system decreases dramatically when Rx moves far away from Tx. In Fig. 8(b), a negative permeability metamaterial slab can effectively focus the magnetic flux lines towards Rx, thereby improving the efficiency of WPT system. Based on this principle, many studies have been conducted to use magnetic metamaterials for WPT with various architectures and dimensions.

3.3. Magnetoinductive wave (MIW) in metamaterial array

Magnetic metamaterials can support a slow wave known as magneto-inductive waves (MIWs) [88 - 90], which are generated as a result of inter-element coupling between periodically arranged unit cells [91 - 94]. Various physical phenomena associated with MIWs, such as negative refraction, and backward propagation, were investigated by Solymar and Shamonina [95]. The simplest embodiment of the magnetic metamaterial waveguides is the design of a finite array of loops loaded with capacitors, as shown in Fig. 9.

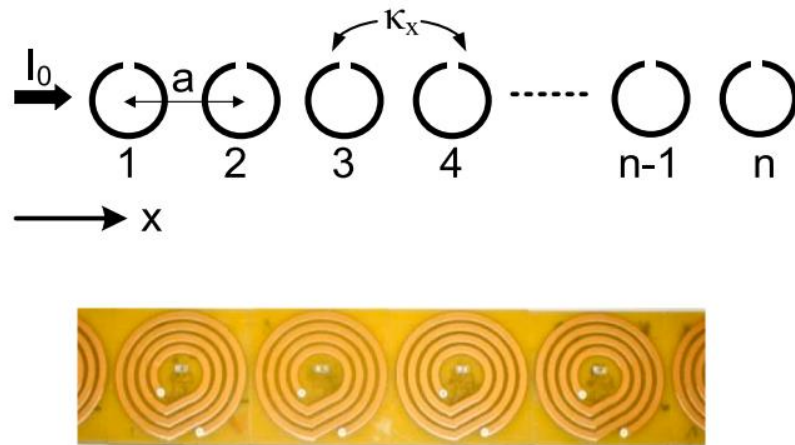


Figure 9. Schematic and photographs of the resonator-coupled array [96]. Copyright 2019 Elsevier.

We can apply Kirchhoff's law for the voltage induced in the loops while only considering the nearest neighbor's coupling. We can derive the dispersion relationship for the array [97]:

$$1 - \frac{\omega_0^2}{\omega^2} + \kappa \cos(\beta a) \cosh(\alpha a) = 0 \quad (22)$$

$$\frac{1}{Q} - \kappa \sin(\beta a) \sinh(\alpha a) = 0$$

where β is the propagation constant of the wave traveling in the array and α is the attenuation coefficient per length. $\kappa = 2M/L$ is the coupling coefficient between two neighbor elements and Q is the quality factor of the element defined as $\omega L/R$.

Due to the low losses in MM unit cell, the element achieves a very high Q-factor then $\cosh(\alpha a) = 1$, $\sinh(\alpha a) = \alpha a$. The expression of the propagation constant and attenuation can be given by:

$$\beta = \frac{1}{a} \arccos\left(\frac{\omega_0^2/\omega^2 - 1}{\kappa}\right) \quad (23)$$

$$\alpha a = \frac{1}{\kappa Q \sin(\beta a)} \quad (24)$$

The attenuation per length of the array shows the minimum value at the resonant frequency ω_0 and increases when frequency approaches the edge of the band where $\beta a = 0$ or π .

4. METAMATERIAL-BASED WIRELESS POWER TRANSFER SYSTEM

4.1. Improving transfer efficiency

Transfer efficiency is one of the essential factors of a WPT system. Many researches have been conducted on using metamaterials to increase the WPT efficiency [98 - 100]. Wang *et al.* conducted the first experiment using a metamaterial in WPT with a metamaterial slab having 9×9 unit cells in the plane and a total size of 58.5×58.5 cm [101]. Figure 10(a) shows the original WPT system at a distance of 50 cm. The maximum efficiency for this configuration is about

17 %, as seen in Fig. 10(d). Figures 10(b) and 10(c) illustrate the 3-D metamaterial structure and anisotropic metamaterial slab being inserted in the middle of the transmitter and receiver of WPT system, respectively. In these configurations, the WPT system's peak efficiencies reach 35 % for the 3-D metamaterial structure and 47 % for the anisotropic metamaterial slab. In this design, the improvement in transfer efficiency can be explained by the amplification of the evanescent wave achieved by the metamaterial structure in the middle of the transmitter and receiver. The magnetic field generated from the transmitter coil is mainly in the direction along the axis of the coil. Therefore, it is more efficient to use an anisotropic metamaterial slab with negative permeability in this direction than a 3-D metamaterial structure.

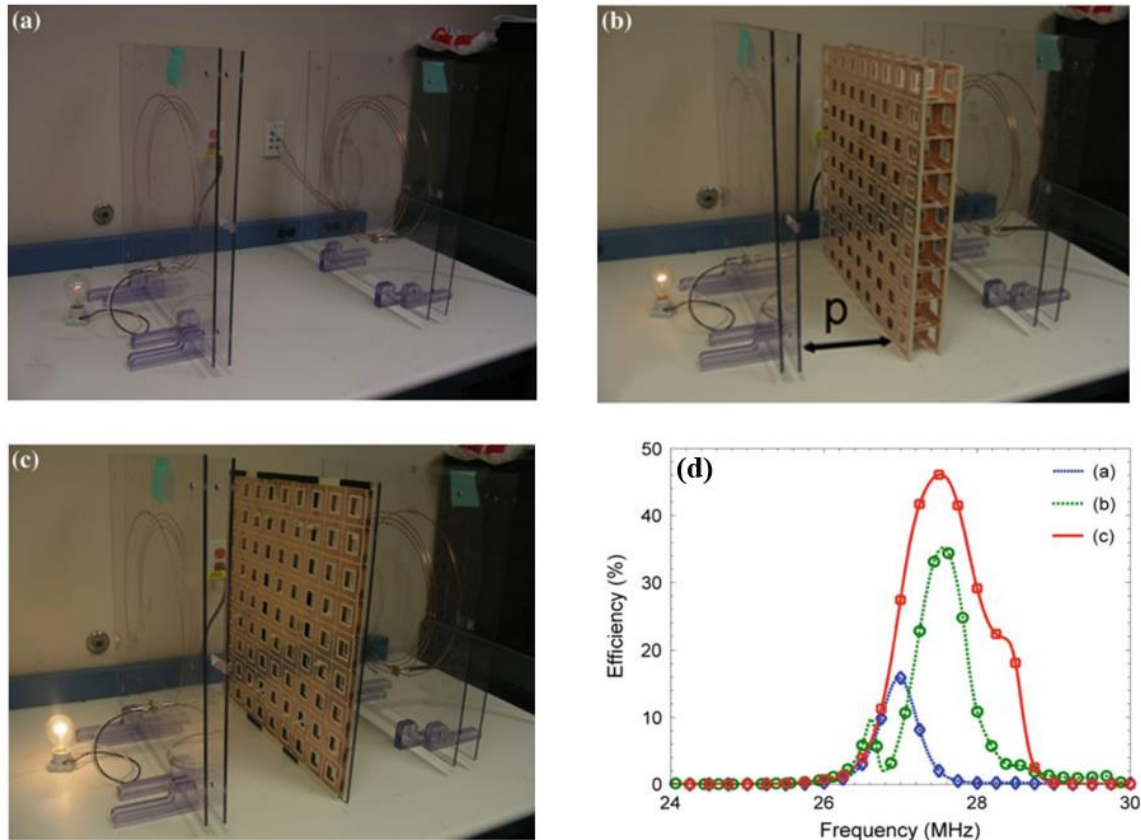


Figure 10. Experiment of WPT with a 40 W light bulb. (a) Original system, (b) with 3-D metamaterial, (c) with anisotropic metamaterial, and (d) the comparison of transfer efficiency for three configurations [101]. Copyright 2016 Mitsubishi Electric Research Laboratories, Inc.

The MM structure can be applied to the WPT system in many other configurations. In [84], the position of the MM slab for achieving maximum transfer efficiency was investigated. MM unit cells were considered as ultra-subwavelength meta-atoms in [102]. The compact metamaterial working at low-frequency (3 MHz) was designed in [103]. A metamaterial-based WPT system that achieved a high transfer efficiency of 85.2 % at the critical coupling point was proposed by Chen *et al.* [104]. An asymmetric mid-range WPT system with metamaterials that had different transmitter and receiver coils was developed by Zeng *et al.* [105]. Various other approaches to using the MM structure have been realized to extend the applicability of the WPT system [106 - 108].

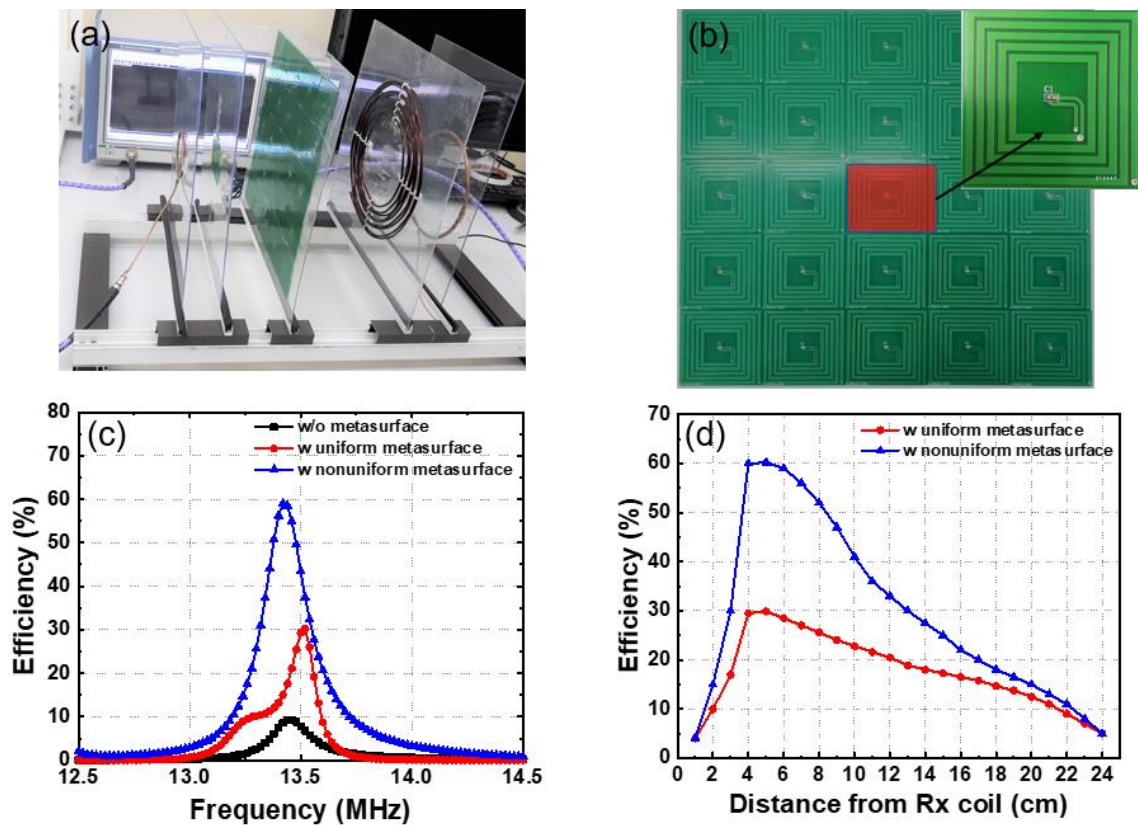


Figure 11. (a) Asymmetric WPT system, (b) 5×5 unit cells metamaterial slab, (c) Measured efficiency of asymmetric WPT system in different configurations, (d) Measured WPT efficiency with various distances from metamaterial slab to receiver resonator [109]. Copyright 2020 Springer Nature.

The asymmetric WPT system with a non-uniform metamaterial slab has been designed by Pham *et al.* [109]. Figures 11(a,b) show the asymmetric WPT system and metamaterial slab constructed by 5×5 unit cells. The total size of the metamaterial slab is 25×25 cm, and the distance between the transmitter and the receiver is 20 cm. The measured efficiencies of WPT in three different configurations (without metamaterial slab, with uniform metamaterial slab, and with non-uniform metamaterial slab) are shown in Fig. 11(c). The peak efficiencies of the three configurations are 9.8 %, 29.9 %, and 60.2 %, respectively. The results demonstrate that the non-uniform metamaterial slab has the ability to enhance the efficiency of the asymmetric WPT system by two times compared to the uniform metamaterial slab. The dependence of WPT performance on the position of the metamaterial slab is investigated and illustrated in Fig. 11(d). There is a position of 4 cm from the receiver to obtain maximum efficiency for both uniform and non-uniform metamaterial slabs. The coupling will be reduced when the distance between the receiver and metamaterial is greater than 4 cm and become over-coupling at shorter distances.

4.2. Misalignment compensation

Misalignment between Tx and Rx coils is an important factor that determines the performance of a WPT system. Lateral or angular misalignments result in a significant reduction in WPT efficiency [110]. Metamaterials are a potential candidate to compensate for the degradation caused by misalignment in the WPT system [105]. Figure 12 shows the H -field

distribution at 6.6 MHz operation frequency of the WPT system with and without the MM slab under a lateral misalignment of 30 cm and an angular misalignment of 45° with a transfer distance of $d = 100$ cm. The results indicate that the MM slab allows the coupling of the evanescent waves, leading to an increase in the magnetic coupling between Tx and Rx of the WPT system. The simulations and experiments in [111] show that the MM slab can compensate for the effect of misalignment on transfer efficiency. For the lateral misalignment of 30 cm, the transfer efficiencies with and without the metamaterial slab are 19 % to 50 %, respectively, corresponding to 31 % of increment. For the angular misalignment of 45° , the transfer efficiency increased by 30.9 % when the MM slab appeared.

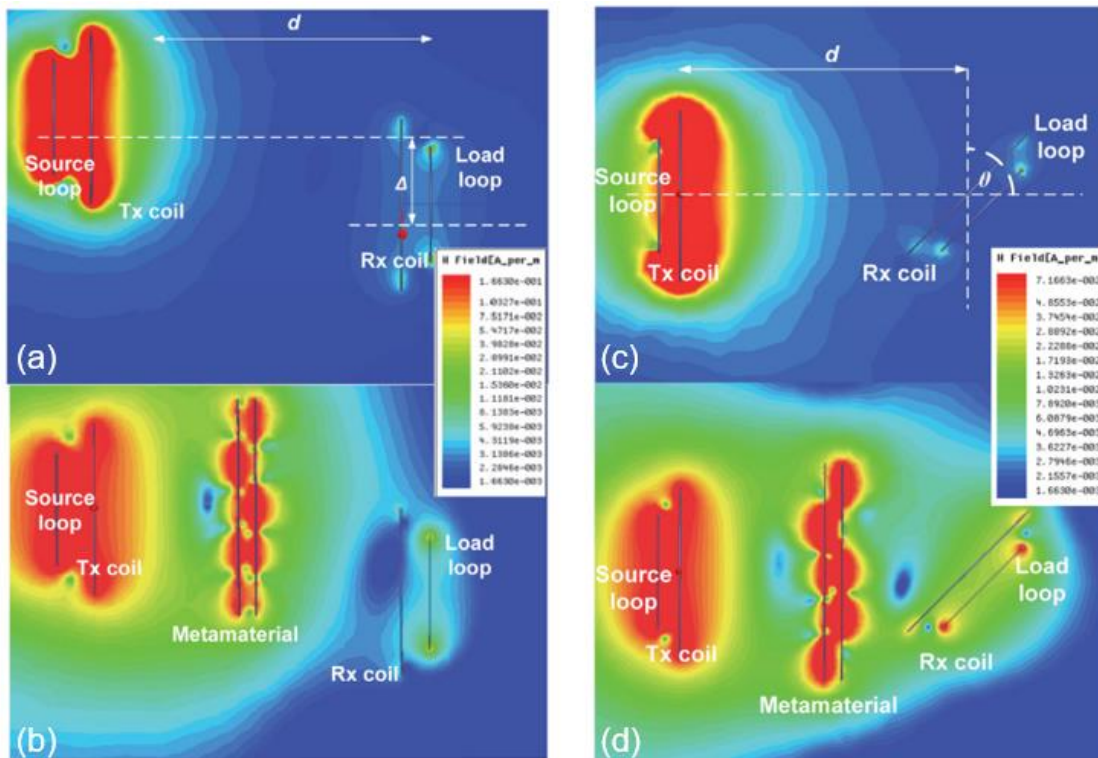


Figure 12. H -field distribution in the WPT system when the Tx and Rx coils are misaligned: (a) original WPT system under lateral misalignment, (b) WPT system with metamaterial slab under lateral misalignment, (c) original WPT system under angular misalignment, (d) WPT system with metamaterial slab under angular misalignment [111]. Copyright 2015 IOP Publishing.

Wang *et al.* also investigated the improvement of the stability of the misalignment WPT system by negative permeability MM slabs [112]. The efficiency of the WPT system could be maintained above 45 % when misalignment occurred. Meanwhile, under the same conditions, the transfer efficiency of the WPT system was as low as 30 % at lateral misalignment and less than 25 % at an angle change. The tunable MM slab for enhancing the transfer efficiency of misaligned WPT has been proposed in [113]. These works have proved that the MM slab can be applied to compensate for the impact of the misalignment on the WPT system, thereby, increasing its application range.

4.3. Leakage magnetic field reduction

The transfer efficiency of the WPT system depends on the magnetic field strength. The large electromagnetic field generated by the wireless charging system can affect electronic components and cause harms to people. Therefore, electromagnetic field pollution needs to be considered in WPT. An effective method is to use shielding materials, such as metallic plates [114]. However, the shielding with the bulky structure is heavy and not aesthetic. To overcome the disadvantages of bulky materials, metamaterial structures were applied to WPT systems for reducing the leakage field in various configurations [115-121]. Lipworth *et al.* designed a shielding plate for the WPT system using a mu-near-zero (MNZ) metamaterial at 13.56 MHz [115]. Lu *et al.* also used the MNZ metamaterial to shield the magnetic field at a specific frequency range of 13.56 MHz [116]. The metasurface has been used to reduce the electric field leakage for near-field WPT [117].

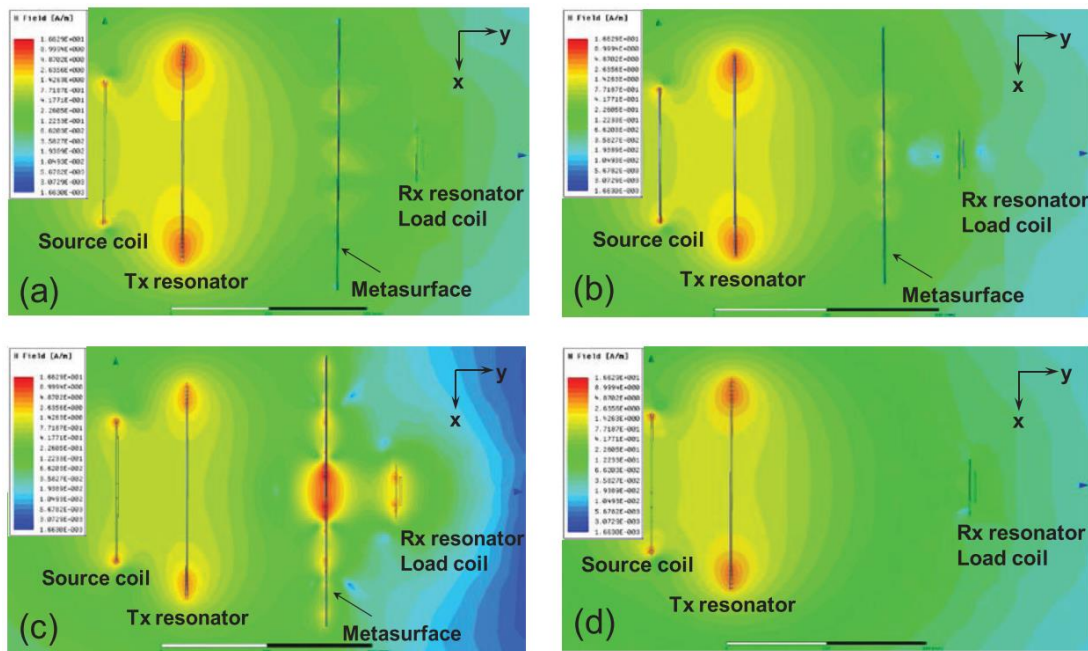


Figure 13. H -field distribution in the WPT system (a) with homogeneous MM slab resonating at $\omega_0 = 6.5$ MHz, (b) with non-homogeneous MM slab resonating at $1.1\omega_0$ except for a center cell, (c) with non-homogeneous MM slab resonating at $0.9\omega_0$ except for a center cell, (d) through free space [122].
Copyright 2015 IOP Publishing.

The homogeneous magnetic MM slab with cavities can localize the magnetic field into a small area and suppress the field in the rest of the slab, thus improving the WPT efficiency and reducing the leakage field [122]. Figure 13 compares the H -field distribution at 6.5 MHz in a WPT system with four configurations: Fig. 13(a) with homogeneous MM slab resonating at $\omega_0 = 6.5$ MHz, Fig. 12(b) with non-homogeneous MM slab resonating at $1.1\omega_0$ except for a center cell, Fig. 13(c) with non-homogeneous MM slab resonating at $0.9\omega_0$ except for a center cell, Fig. 13(d) for original WPT system via free space. When a homogeneous MM slab is inserted, surface waves appear on the MM slab due to MIW propagation, indicating that the MM slab increases the H -field intensity around the receiver. When a non-homogeneous MM slab is added, a cavity is formed, therefore, the H -field is suppressed or enhanced at the original resonant frequency depending on the resonant frequency of MM unit cell in the slab, except for the center cell, which always resonates at 6.5 MHz. In the case of constructive cavity, we observe a very

strong H -field intensity at the cavity location. The H -field is confined to a small area around the cavity region, leading to significantly improved wireless power transmission.

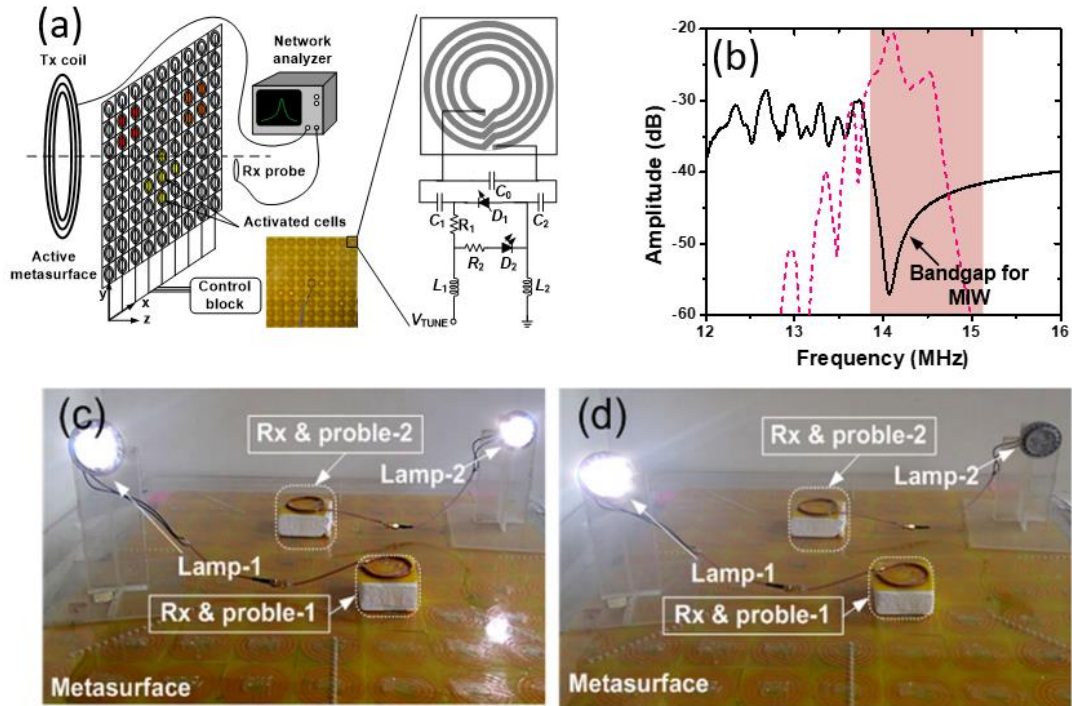


Figure 14. (a) A schematic and photo of the active metasurface with the active unit cell, (b) transmission in two cases: uniform and non-uniform metasurfaces, (c) two receiver LED lamps on metasurface, (d) single selected receiver [123].

An active metasurface constructed from unit cells that can tune the resonant frequency has been designed by Ranaweera *et al.* [123], as shown in Fig. 14. This active metasurface can be applied for WPT to control the magnetic field localizing in selective areas and suppress in the rest of the metasurface. The metasurface consists of 9×9 arrays of unit cells that are individually controlled by a tuning circuit embedded in the backside, as shown in Fig. 14(a). The transmission of uniform and non-uniform metasurfaces is illustrated in Fig. 14(b), which explains the cavity operation mechanism. The cavity is a unit cell whose resonant frequency lies in the hybridization bandgap of the metasurface. Figures 14(c,d) show the experimental results with the use of an active metasurface and two LED lamps. Using the tuning circuit, the cavity location can be selected to control the wireless power link.

5. PERSPECTIVES AND CHALLENGES

It has been shown that metamaterials can improve the WPT efficiency and transfer distance. The development of metamaterials will have a positive impact on WPT systems. However, the investigation for applying metamaterials to WPT systems is still very primitive. There are numerous directions for further development of metamaterial-based WPT systems.

5.1. Reducing the size and weight of metamaterial-based WPT systems

The total size of resonator coils and metamaterial slab are still considerably large [84]. In some cases, it is not practical for many applications. Large size also wastes material and increases production costs. Therefore, miniaturization and lightweight are needed to increase the application range of metamaterial-based WPT systems. Optimal design of structural configurations, new material for fabrication and other effective methods can be used for this purpose.

5.2. Multi-band frequency

The ISM (Industrial, Scientific and Medical) frequency band for industrial, scientific and medical use is defined by the ITU (International Telecommunication Union) Radiocommunication Sector. Meanwhile, the industry of Alliance for Wireless Power (A4WP), Wireless Power Consortium (WPC), and Power Meters Alliance (PMA) propose the operation frequency range of WPT systems [30]. The incompatibility of these standards poses challenges to the development of WPT. Multi-band frequency band WPT is a solution to this problem. Furthermore, many previous works have extensively studied multi-band metamaterials at microwave frequencies. The results obtained can be partially applied to the MHz frequency band. However, studies of multi-band metamaterials at MHz frequency need to be carried out.

5.3. Low-frequency metamaterials and increased transfer power

The properties of metamaterials operating at MHz frequency have been discussed in many works. However, high frequencies pose significant challenges to efficient switching converters. Therefore, it is suitable for low transfer power. Reducing the operating frequency of metamaterials and applying to kHz range WPT is one direction for high transfer power systems.

5.4. Active metamaterial devices for WPT

Recently, active metamaterial slabs which can tune their properties by external capacitors have been proposed [121]. A transmission link can be created in the metamaterial slab by modifying the resonant frequency of metamaterial unit cells. Using the transmission link, both power transfer efficiency and safety can be improved. These metamaterial devices have great potential for smart table applications, where all electronic devices can be charged at any position on the table. However, the transmission link only exists in the 2-D plane, which is a limit of this configuration. Therefore, the research to create a 3-D transmission link for improving the application range of metamaterial devices is a promising direction.

5.5. Human safety

Electromagnetic exposure is a critical problem that needs to be considered for electric systems. Electromagnetic metamaterials can also be used to reduce or block all electromagnetic leakage. Therefore, studies on using metamaterials for focusing or shielding electromagnetic waves are also an inevitable tendency.

6. CONCLUSIONS

This paper has reviewed the current status of WPT systems and the advantages of using metamaterials to improve these systems' performance. Brief history and fundamentals of WPT

systems and metamaterials have been introduced. The advantages and disadvantages of three types of WPT have been reviewed in Section 2. The near-field WPT provides most of the applications in human life, therefore, Section 3 and Section 4 focus on using metamaterials to improve the limit of near-field WPT systems. The perspective and challenges of metamaterial-based WPT have been discussed in Section 5. Metamaterials with the evanescent wave amplification characteristic could be used for enhancing the transfer efficiency, compensating for the impact of misalignment between transmitter and receiver, and localizing the magnetic field into a small region to select the wireless power transmission locations. Electromagnetic exposure is a concern when applying WPT systems in real life. Several metamaterial structures can be used as shielding plates or creating cavities to reduce the leakage of the magnetic field. This review is expected to offer insight into understanding the trends of using metamaterials to improve WPT performance. The negative permeability metamaterial structures have huge potential for the future development of WPT applications.

Acknowledgements. This research is funded by Vietnam Academy of Science and Technology (VAST) under grant number “VAST03.01/21-22”.

CRedit authorship contribution statement. Thanh Son Pham: Methodology, Writing manuscript. Bui Xuan Khuyen: Formal analysis. Bui Son Tung: Formal analysis. Le Thi Hong Hiep: Investigation. Vu Dinh Lam: Supervision.

Declaration of competing interest. The authors declare that they have no known competing financial interests or personal relationships that could have appeared to influence the work reported in this paper.

REFERENCES

1. Song M, Jayathurathnage P., Zanganeh E., Krasikova M., Smirnov P., Belov P., Kapitanova P., Simovski C., Tretyakov S., Krasnok A. - Wireless power transfer based on novel physical concepts, *Nat. Electron.* **4** (2021) 707-716. <https://doi.org/10.1038/s41928-021-00658-x>.
2. Song M., Belov P., Kapitanova P. - Wireless power transfer inspired by the modern trends in electromagnetics, *Appl. Phys. Rev.* **4** (2017) 1-19. <https://doi.org/10.1063/1.4981396>.
3. Shinohara N. - Power without wires, *IEEE Microw. Mag.* **12** (2011) S64-S73. <https://doi.org/10.1109/MMM.2011.942732>.
4. Tesla N. - Apparatus for transmitting electrical energy, 1119732, 1914.
5. Brown W. C. - Adapting microwave techniques to help solve future energy problems, *IEEE Trans. Microw. Theory Tech.* **MTT-21** (1973) 753-763. <https://doi.org/10.1109/GMTT.1973.1123144>.
6. Matsumoto H. - Research on solar power satellites and microwave power transmission in Japan, *IEEE Microw. Mag.* **3** (2002) 36–45. <https://doi.org/10.1109/MMW.2002.1145674>.
7. Kesler M. - Highly resonant wireless power transfer: safe, efficient, and over distance, 2013. <http://www.witricity.com/pdfs/highly-resonant-power-transfer-kesler-witricity-2013.pdf>.
8. Hui S. Y. - Planar wireless charging technology for portable electronic products and Qi, *Proc. IEEE.* **101** (2013) 1290-1301. <https://doi.org/10.1109/JPROC.2013.2246531>.
9. Mayordomo I., Drager T., Spies P., Bernhard J., Pflaum A. - An overview of technical challenges and advances of inductive wireless power transmission, *Proc. IEEE.* **101**

- (2013) 1302-1311. <https://doi.org/10.1109/JPROC.2013.2243691>.
10. Ha-Van N., Le-Huu H., Le M. T., Park K., Seo C. - Free-positioning wireless power transfer using a 3D transmitting coil for portable devices, *J. Electromagn Eng Sci.* **20** (2020) 270-276. <https://doi.org/10.26866/jees.2020.20.4.270>.
 11. Park J., Park C., Shin Y., Kim D., Park B., Cho J., Choi J., Ahn S. - Planar multiresonance reactive shield for reducing electromagnetic interference in portable wireless power charging application, *Appl. Phys. Lett.* **114** (2019). <https://doi.org/10.1063/1.5097038>.
 12. Alhamrouni I., Iskandar M., Salem M., Awal L. J., Jusoh A., Sutikno T. - Application of inductive coupling for wireless power transfer, *Int. J. Power Electron. Drive Syst.* **11** (2020) 1109-1116.
 13. Zhou H., Zhu B., Hu W., Liu Z., Gao X. - Modelling and practical implementation of 2-Coil wireless power transfer systems, *J. Electr. Comput. Eng.* **2014** (2014) 1-8. <https://doi.org/10.1155/2014/906537>.
 14. Lee W. S., Oh K.-S., Yu J. W. - Distance-insensitive wireless power transfer and near-field communication using a current-controlled loop with a loaded capacitance, *IEEE Trans. Antennas Propag.* **62** (2014) 936-940. <https://doi.org/10.1109/TAP.2013.2290549>.
 15. Wei X., Wang Z., Dai H. - A critical review of wireless power transfer via strongly coupled magnetic resonances, *Energies.* **7** (2014) 4316-4341. <https://doi.org/10.3390/en7074316>.
 16. Bevacqua M. T., Bellizzi G. G., Merenda M. - An efficient far-field wireless power transfer via field intensity shaping techniques, *Electronics.* **10** (2021) 1-13. <https://doi.org/10.3390/electronics10141609>.
 17. Brown W. C., Eves E. E. - Beamed microwave power transmission and its application to space, *IEEE Trans. Microw. Theory Tech.* **40** (1992) 1239-1250. <https://doi.org/10.1109/22.141357>.
 18. Lerosey G. - Wireless power on the move, *Nature.* **546** (2017) 354-355. <https://doi.org/10.1038/546354a>.
 19. Moon S., Moon G. - Wireless power transfer system with an asymmetric four-coil resonator for electric vehicle battery chargers, *IEEE Trans. Power Electron.* **31** (2016) 6844-6854. <https://doi.org/10.1109/TPEL.2015.2506779>.
 20. Liu Z., Zhong Z., Guo Y. X. - Rapid design approach of optimal efficiency magnetic resonant wireless power transfer system, *Electron. Lett.* **52** (2016) 314-315. <https://doi.org/https://doi.org/10.1049/el.2015.3571>.
 21. Pokharel R. K., Barakat A., Alshhawy S., Yoshitomi K., Sarris C. - Wireless power transfer system rigid to tissue characteristics using metamaterial inspired geometry for biomedical implant applications, *Sci. Rep.* **11** (2021) 1-10. <https://doi.org/10.1038/s41598-021-84333-3>.
 22. Pham T. S., Nguyen T. D., Tung B. S., Khuyen B. X., Hoang T. T., Ngo Q. M., Hiep L. T. H., Lam V. D. - Optimal frequency for magnetic resonant wireless power transfer in conducting medium, *Sci. Rep.* **11** (2021) 1-11. <https://doi.org/10.1038/s41598-021-98153-y>.
 23. Xu D., Zhang Q., Li X. - Implantable magnetic resonance wireless power transfer system based on 3D flexible coils, *Sustainability.* **12** (2020) 4149. <https://doi.org/10.3390/su12104149>.

24. Assawaworrarit S., Yu X., Fan S. - Robust wireless power transfer using a nonlinear parity-time-symmetric circuit, *Nature*. **546** (2017) 387-390. <https://doi.org/10.1038/nature22404>.
25. Choi J. H., Kang S. H., Jung C. W. - Magnetic resonant wireless power transfer with L-shape arranged resonators for laptop computer, *J. Electromagn. Eng. Sci.* **17** (2017) 126-132. <https://doi.org/10.5515/JKIEES.2017.17.3.126>.
26. Kurs A., Karalis A., Moffatt R., Joannopoulos J. D., Fisher P., Soljačić M. - Wireless power transfer via strongly coupled magnetic resonances, *Science* **317** (2007) 83-86. <https://doi.org/10.1126/science.1143254>.
27. Roberts D. M., Clements A. P., McDonald R., Bobowski J. S., Johnson T. - Mid-range wireless power transfer at 100 MHz using magnetically coupled loop-gap resonators, *IEEE Trans. Microw. Theory Tech.* **69** (2021) 3510-3527. <https://doi.org/10.1109/TMTT.2021.3073133>.
28. Shi L., Rasool N., Zhu H., Huang K., Yang Y. - Design and experiment of a reconfigurable magnetic resonance coupling wireless power transmission system, *IEEE Microw. Wirel. Components Lett.* **30** (2020) 705-708. <https://doi.org/10.1109/LMWC.2020.2997068>.
29. Mollaei M. S. M., Jayathurathnage P., Tretyakov S. A., Simovski C. R. - High-impedance wireless power transfer transmitter coils for freely positioning receivers, *IEEE Access.* **9** (2021) 42994-43000. <https://doi.org/10.1109/ACCESS.2021.3064212>.
30. Huang X., Zhang C., Cong L., Cai R., Yang F., Lu C. - Development and prospects of metamaterial in wireless power transfer, *IET Power Electron.* **14** (2021) 2423-2440. <https://doi.org/https://doi.org/10.1049/pel2.12189>.
31. Lee W., Yoon Y. K. - Wireless power transfer systems using metamaterials: A review, *IEEE Access.* **8** (2020) 147930-147947. <https://doi.org/10.1109/ACCESS.2020.3015176>.
32. Kung M. L., Lin K. H. - Investigation of multi-layer metamaterial for enhancing efficiency of near-field wireless power transfer systems, in: 2018 Prog. Electromagn. Res. Symp., 2018: pp. 2484-2488. <https://doi.org/10.23919/PIERS.2018.8597730>.
33. Sun K., Fan R., Zhang X., Zhang Z., Shi Z., Wang N., Xie P., Wang Z., Fan G., Liu H., Liu C., Li T., Yan C., Guo Z. - An overview of metamaterials and their achievements in wireless power transfer, *J. Mater. Chem. C.* **6** (2018) 2925-2943. <https://doi.org/10.1039/C7TC03384B>.
34. Das R., Basir A., Yoo H. - A metamaterial-coupled wireless power transfer system based on cubic high-dielectric resonators, *IEEE Trans. Ind. Electron.* **66** (2019) 7397-7406. <https://doi.org/10.1109/TIE.2018.2879310>.
35. Rong C., Lu C., Zeng Y., Tao X., Liu X., Liu R., He X., Liu M. - A critical review of metamaterial in wireless power transfer system, *IET Power Electron.* **14** (2021) 1541-1559. <https://doi.org/https://doi.org/10.1049/pel2.12099>.
36. Mi C. C., Buja G., Choi S. Y., Rim C. T. - Modern advances in wireless power transfer systems for roadway powered electric vehicles, *IEEE Trans. Ind. Electron.* **63** (2016) 6533-6545. <https://doi.org/10.1109/TIE.2016.2574993>.
37. Garnica J., Chinga R. A., Lin J. - Wireless power transmission: From far field to near field, *Proc. IEEE.* **101** (2013) 1321-1331. <https://doi.org/10.1109/JPROC.2013.2251411>.
38. Lin J. C. - Space solar-power stations, wireless power transmissions, and biological implications, *IEEE Microw. Mag.* **3** (2002) 36-42. <https://doi.org/10.1109/6668.990673>.

39. Hui S. Y. R., Zhong W., Lee C. K. - A critical review of recent progress in mid-range wireless power transfer, *IEEE Trans. Power Electron.* **29** (2014) 4500-4511. <https://doi.org/10.1109/TPEL.2013.2249670>.
40. Khan H., Ali S. A., Wajid M., Alam M. S. - Antenna array design on flexible substrate for wireless power transfer, *Front. Eng. Built Environ.* **1** (2021) 55-67. <https://doi.org/10.1108/FEBE-03-2021-0018>.
41. Xia M., Aïssa S. - On the efficiency of far-field wireless power transfer, *IEEE Trans. Signal Process.* **63** (2015) 2835-2847. <https://doi.org/10.1109/TSP.2015.2417497>.
42. Zhang Z., Pang H., Georgiadis A., Cecati C. - Wireless power transfer - an overview, *IEEE Trans. Ind. Electron.* **66** (2019) 1044-1058. <https://doi.org/10.1109/TIE.2018.2835378>.
43. Ali A., Yasin M. N. M., Husin M. F. C., Hambali N. A. M. A. - Design and analysis of 2-coil wireless power transfer (WPT) using magnetic coupling technique, *Int. J. Power Electron. Drive Syst.* **10** (2019) 611-616.
44. Alrawashdeh R. - A review on wireless power transfer in free space and conducting lossy media, *Jordanian J. Comput. Inf. Technol.* **03** (2017) 71-88. <https://doi.org/10.5455/jjcit.71-1483030287>.
45. Younesiraad H., Bemani M. - Analysis of coupling between magnetic dipoles enhanced by metasurfaces for wireless power transfer efficiency improvement, *Sci. Rep.* **8** (2018) 1-11. <https://doi.org/10.1038/s41598-018-33174-8>.
46. Chu S., Stevens C. J., Shamonina E. - Wireless power transfer in attenuating media, *AIP Adv.* **11** (2021) 1-7. <https://doi.org/10.1063/5.0059932>.
47. Seo D. W., Lee J. H., Lee H. - Study on two-coil and four-coil wireless power transfer system using Z-parameter approach, *ETRI J.* **38** (2016) 568-578. <https://doi.org/10.4218/etrij.16.0115.0692>.
48. Houran M. A., Yang X., Chen W. - Magnetically coupled resonance WPT: review of compensation topologies, resonator structures with misalignment, and EMI diagnostics, *Electronics.* **7** (2018) 1-45. <https://doi.org/10.3390/electronics7110296>.
49. Zhang X., Meng H., Wei B., Wang S., Yang Q. - An improved three-coil wireless power link to increase spacing distance and power for magnetic resonant coupling system, *EURASIP J. Wirel. Commun. Netw.* **2018** (2018) 1-8. <https://doi.org/10.1186/s13638-018-1148-8>.
50. Pham T. S., Nguyen T. V., Nguyen D. K., Ha T. K. D. - Investigation on coil misalignment affect magnetic resonant wireless power transfer system, *Journal of Military Science and Technology.* **75** (2021) 57-64. (in Vietnamese).
51. Kim D., Kim J., Park Y. - Optimization and design of small circular coils in a magnetically coupled wireless power transfer system in the megahertz frequency, *IEEE Trans. Microw. Theory Tech.* **64** (2016) 2652-2663. <https://doi.org/10.1109/TMTT.2016.2582874>.
52. Kang S. H., Nguyen V. T., Jung C. W. - Analysis of MR-WPT using planar textile resonators for wearable applications, *IET Microwaves, Antennas Propag.* **10** (2016) 1541-1546. <https://doi.org/https://doi.org/10.1049/iet-map.2016.0024>.
53. Liu X., Wang G. - A novel wireless power transfer system with double intermediate resonant coils, *IEEE Trans. Ind. Electron.* **63** (2016) 2174-2180. <https://doi.org/>

- 10.1109/TIE.2015.2510512.
54. Zhang Y., Zhao Z. - Frequency splitting analysis of two-coil resonant wireless power transfer, *IEEE Antennas Wirel. Propag. Lett.* **13** (2014) 400-402. <https://doi.org/10.1109/LAWP.2014.2307924>.
 55. Ishizaki T., Komori T., Ishida T., Awai I. - Comparative study of coil resonators for wireless power transfer system in terms of transfer loss, *IEICE Electron. Express.* **7** (2010) 785-790. <https://doi.org/10.1587/elex.7.785>.
 56. Kang S. H., Park S., Jung C. W. - Textile resonators using a sintered metal conductor for wearable MR-WPT with high efficiency and wearability, *Microw. Opt. Technol. Lett.* **59** (2017) 668-672. <https://doi.org/https://doi.org/10.1002/mop.30363>.
 57. Sample A. P., Meyer D. T., Smith J. R. - Analysis, experimental results, and range adaptation of magnetically coupled resonators for wireless power transfer, *IEEE Trans. Ind. Electron.* **58** (2011) 544-554. <https://doi.org/10.1109/TIE.2010.2046002>.
 58. Sample A. P., Waters B. H., Wisdom S. T., Smith J. R. - Enabling seamless wireless power delivery in dynamic environments, *Proc. IEEE.* **101** (2013) 1343-1358. <https://doi.org/10.1109/JPROC.2013.2252453>.
 59. Veselago V. G. - The electrodynamics of substances with simultaneously negative values of epsilon and mu, *Sov. Phys. Uspekhi.* **10** (1968) 509-514. <https://doi.org/10.1070/pu1968v010n04abeh003699>.
 60. Pendry J. B., Holden A. J., Stewart W. J., Youngs I. - Extremely low frequency plasmons in metallic mesostructures, *Phys. Rev. Lett.* **76** (1996) 4773-4776.
 61. Pendry J. B., Holden A. J., Robbins D. J., Stewart W. J. - Magnetism from conductors and enhanced nonlinear phenomena, *IEEE Trans. Microw. Theory Tech.* **47** (1999) 2075-2084. <https://doi.org/10.1109/22.798002>.
 62. Rao S., Ong K. - Amplification of evanescent waves in a lossy left-handed material slab, *Phys. Rev. B - Condens. Matter Mater. Phys.* **68** (2003) 1-4. <https://doi.org/10.1103/PhysRevB.68.113103>.
 63. Smith D. R., Padilla W. J., Vier D. C., Nemat-Nasser S. C., Schultz S. - Composite medium with simultaneously negative permeability and permittivity, *Phys. Rev. Lett.* **84** (2000) 4184-4187. <https://doi.org/10.1103/PhysRevLett.84.4184>.
 64. Pendry J. B. - Negative refraction, *Contemp. Phys.* **45** (2004) 191-202. <https://doi.org/10.1080/00107510410001667434>.
 65. Nguyen H. T., Bui T. S., Yan S., Vandenbosch G. A. E., Lievens P., Vu L. D., E. Janssens - Broadband negative refractive index obtained by plasmonic hybridization in metamaterials, *Appl. Phys. Lett.* **109** (2016) 1-5. <https://doi.org/10.1063/1.4968802>.
 66. Tung B. S., Khuyen B. X., Linh P. T., Tung N. T., Manh D. H., Lam V. D. - Polarization-insensitive electromagnetically-induced transparency in planar metamaterial based on coupling of ring and zigzag spiral resonators, *Mod. Phys. Lett. B.* **34** (2020) 2050093. <https://doi.org/10.1142/S0217984920500931>.
 67. Almoneef T. S., Ramahi O. M. - Metamaterial electromagnetic energy harvester with near unity efficiency, *Appl. Phys. Lett.* **106** (2015) 1-4. <https://doi.org/10.1063/1.4916232>.
 68. Khuyen B. X., Tung B. S., Dung N. V., Yoo Y. J., Kim Y. J., Kim K. W., Lam V. D., Yang J. G., Lee Y. - Size-efficient metamaterial absorber at low frequencies: Design,

- fabrication, and characterization, *J. Appl. Phys.* **117** (2015) 1-7. <https://doi.org/10.1063/1.4923053>.
69. Tiep D. H., Khuyen B. X., Tung B. S., Kim Y. J., Hwang J. S., Lam V. D., Lee Y. P. - Enhanced-bandwidth perfect absorption based on a hybrid metamaterial, *Opt. Mater. Express*. **8** (2018) 2751-2759. <https://doi.org/10.1364/OME.8.002751>.
 70. Khuyen B. X., Tung B. S., Yoo Y. J., Kim Y. J., Kim K. W., Chen L. Y., Lam V. D., Lee Y. - Miniaturization for ultrathin metamaterial perfect absorber in the VHF band, *Sci. Rep.* **7** (2017) 1-7. <https://doi.org/10.1038/srep45151>.
 71. Ha D. T., Tung B. S., Khuyen B. X., Pham T. S., Tung N. T., Tung N. H., Hoa N. T., Lam V. D., Zheng H., Chen L., Lee Y. - Dual-band, polarization-insensitive, ultrathin and flexible metamaterial absorber based on high-order magnetic resonance, *Photonics* **8** (2021) 574. <https://doi.org/10.3390/photonics8120574>.
 72. Long L. V., Khiem N. S., Tung B. S., Tung N. T., Giang T. T., Son P. T., Khuyen B. X., Lam V. D., Chen L., Zheng H., Lee Y. - Flexible broadband metamaterial perfect absorber based on graphene-conductive inks, *Photonics*. **8** (2021) 440. <https://doi.org/10.3390/photonics8100440>.
 73. Singh G., Ni R., Marwaha A. - A review of metamaterials and its applications, *Int. J. Eng. Trends Technol.* **19** (2015) 305-310. <https://doi.org/10.14445/22315381/ijett-v19p254>.
 74. Bui T. S., Dao T. D., Dang L. H., Vu L. D., Ohi A., Nabatame T., Lee Y., Nagao T., Hoang C. V. - Metamaterial-enhanced vibrational absorption spectroscopy for the detection of protein molecules, *Sci. Rep.* **6** (2016) 1-7. <https://doi.org/10.1038/srep32123>.
 75. Ha D. T., Dzung N. D., Ngoc N. V., Tung B. S., Pham T. S., Lee Y., Chen L. Y., Khuyen B. X., Lam V. D. - Switching between perfect absorption and polarization conversion, based on hybrid metamaterial in the GHz and THz bands, *J. Phys. D. Appl. Phys.* **54** (2021) 1-10. <https://doi.org/10.1088/1361-6463/abeb97>.
 76. Nguyen T. H., Bui S. T., Nguyen X. C., Vu D. L., Bui X. K. - Tunable broadband-negative-permeability metamaterials by hybridization at THz frequencies, *RSC Adv.* **10** (2020) 28343-28350. <https://doi.org/10.1039/D0RA04612D>.
 77. Radkovskaya A., Petrov P., Kiriushchikina S., Satskiy A., Ivanyukovich M., Vakulenko A., Prudnikov V., Kotelnikova O., Korolev A., Zakharov P. - Magnetic metamaterials: Coupling and permeability, *J. Magn. Magn. Mater.* **459** (2018) 187-190. <https://doi.org/10.1016/j.jmmm.2017.11.031>.
 78. Zhang Y., Tang H., Yao C., Li Y., Xiao S. - Experiments on adjustable magnetic metamaterials applied in megahertz wireless power transmission, *AIP Adv.* **5** (2015) 1-9. <https://doi.org/10.1063/1.4907043>.
 79. Smith D. R., Schultz S., Markoš P., Soukoulis C. M. - Determination of effective permittivity and permeability of metamaterials from reflection and transmission coefficients, *Phys. Rev. B.* **65** (2002) 1-5. <https://doi.org/10.1103/PhysRevB.65.195104>.
 80. Smith D. R., Vier D. C., Koschny T., Soukoulis C. M. - Electromagnetic parameter retrieval from inhomogeneous metamaterials, *Phys. Rev. E.* **71** (2005) 1-11. <https://doi.org/10.1103/PhysRevE.71.036617>.
 81. Rothwell E. J., Frasch J. L., Ellison S. M., Chahal P., Ouedraogo R. O. - Analysis of the Nicolson-Ross-Weir method for characterizing the electromagnetic properties of engineered materials, *Prog. Electromagn. Res.* **157** (2016) 31-47. <https://doi.org/>

- 10.2528/PIER16071706.
82. Chen X., Grzegorzczak T. M., Wu B. I., Pacheco J., Kong J. A. - Robust method to retrieve the constitutive effective parameters of metamaterials, *Phys. Rev. E.* **70** (2004) 1-7. <https://doi.org/10.1103/PhysRevE.70.016608>.
 83. Pham T. S., Nguyen T. D., Vu D. L. - Metamaterials for improving efficiency of magnetic resonant wireless power transfer applications, *Commun. Phys.* **32** (2022) 1-8.
 84. Ranaweera A. L. A. K., Duong T. P., Lee J. W. - Experimental investigation of compact metamaterial for high efficiency mid-range wireless power transfer applications, *J. Appl. Phys.* **116** (2014) 1-8. <https://doi.org/10.1063/1.4891715>.
 85. Harris W. C., Stancil D. D., Ricketts D. S. - Improved wireless power transfer efficiency with non-perfect lenses, *Appl. Phys. Lett.* **114** (2019) 1-4. <https://doi.org/10.1063/1.5081629>.
 86. Zhao Y. - Evanescent wave amplification and subwavelength imaging by ultrathin uniaxial μ -near-zero material, *AIP Adv.* **4** (2014) 1-6. <https://doi.org/10.1063/1.4866579>.
 87. Lee W., Yoon Y. K. - Rollable metamaterial screen for magnetic resonance coupling-based high-efficiency wireless power transfer, *Int. J. Microw. Wirel. Technol.* **13** (2021) 365-373. <https://doi.org/DOI:10.1017/S1759078720001221>.
 88. Shamonina E., Kalinin V. A., Ringhofer K. H., Solymar L. - Magneto-inductive waveguide, *Electron. Lett.* **38** (2002) 371-373. <https://doi.org/10.1049/el:20020258>.
 89. Chu S., Luloff M. S., Yan J., Petrov P., Stevens C. J., Shamonina E. - Magnetoinductive waves in attenuating media, *Sci. Rep.* **11** (2021) 1-12. <https://doi.org/10.1038/s41598-021-85838-7>.
 90. Sandoval F. S., Delgado S. M. T., Moazenzadeh A., Wallrabe U. - A 2-D magnetoinductive wave device for freer wireless power transfer, *IEEE Trans. Power Electron.* **34** (2019) 10433-10445. <https://doi.org/10.1109/TPEL.2019.2904875>.
 91. Shamonina E., Kalinin V. A., Ringhofer K. H., Solymar L. - Magnetoinductive waves in one, two, three dimensions, *J. Appl. Phys.* **92** (2002) 6252-6261. <https://doi.org/10.1063/1.1510945>.
 92. Yang F., Song J., Guo Z., Wu X., Zhu K., Jiang J., Sun Y., Jiang H., Li Y., Chen H. - Actively controlled asymmetric edge states for directional wireless power transfer, *Opt. Express.* **29** (2021) 7844-7857. <https://doi.org/10.1364/OE.417887>.
 93. Song J., Yang F., Guo Z., Wu X., Zhu K., Jiang J., Sun Y., Li Y., Jiang H., Chen H. - Wireless power transfer via topological modes in dimer chains, *Phys. Rev. Appl.* **15** (2021) 1-13. <https://doi.org/10.1103/PhysRevApplied.15.014009>.
 94. Feis J., Stevens C. J., Shamonina E. - Wireless power transfer through asymmetric topological edge states in diatomic chains of coupled meta-atoms, *Appl. Phys. Lett.* **117** (2020) 1-6. <https://doi.org/10.1063/5.0024077>.
 95. Syms R. R. A., Shamonina E., Solymar L. - Positive and negative refraction of magnetoinductive waves in two dimensions, *Eur. Phys. J. B. Condens. Matter Complex Syst.* **46** (2005) 301-308. <https://doi.org/10.1140/epjb/e2005-00253-9>.
 96. Pham T. S., Bui H. N., Lee J. W. - Wave propagation control and switching for wireless power transfer using tunable 2-D magnetic metamaterials, *J. Magn. Magn. Mater.* **485** (2019) 126-135. <https://doi.org/10.1016/j.jmmm.2019.04.034>.

97. Sydoruk O., Zhuromskyy O., Shamonina E., Solymar L. - Phonon-like dispersion curves of magnetoinductive waves, *Appl. Phys. Lett.* **87** (2005) 1-3. <https://doi.org/10.1063/1.2011789>.
98. Younesiraad H., Bemani M., Matekovits L. - Optimal Huygens' metasurface for wireless power transfer efficiency improvement, *IEEE Access.* **8** (2020) 216409-216418. <https://doi.org/10.1109/ACCESS.2020.3041337>.
99. Rong C., Tao X., Lu C., Hu Z., Huang X., Zeng Y., Liu M. - Analysis and optimized design of metamaterials for mid-range wireless power transfer using a class-E RF power amplifier, *Appl. Sci.* **9** (2019) 1-14. <https://doi.org/10.3390/app9010026>.
100. Song M., Baryshnikova K., Markvart A., Belov P., Nenasheva E., Simovski C., Kapitanova P. - Smart table based on a metasurface for wireless power transfer, *Phys. Rev. Appl.* **11** (2019) 1-9. <https://doi.org/10.1103/PhysRevApplied.11.054046>.
101. Wang B., Teo K. H., Nishino T., Yerazunis W., Barnwell J., Zhang J. - Experiments on wireless power transfer with metamaterials, *Appl. Phys. Lett.* **98** (2011) 1-4. <https://doi.org/10.1063/1.3601927>.
102. Wu Q., Li Y. H., Gao N., Yang F., Chen Y. Q., Fang K., Zhang Y. W., Chen H. - Wireless power transfer based on magnetic metamaterials consisting of assembled ultra-subwavelength meta-atoms, *EPL (Europhysics Lett.)* **109** (2015) 1-6. <https://doi.org/10.1209/0295-5075/109/68005>.
103. Rodríguez E. S. G., RamRakhyani A. K., Schurig D., Lazzi G. - Compact low-frequency metamaterial design for wireless power transfer efficiency enhancement, *IEEE Trans. Microw. Theory Tech.* **64** (2016) 1644-1654. <https://doi.org/10.1109/TMTT.2016.2549526>.
104. Chen J., Ding Z., Hu Z., Wang S., Cheng Y., Liu M., Wei B., Wang S. - Metamaterial-based high-efficiency wireless power transfer system at 13.56 Mhz for low power applications, *Prog. Electromagn. Res. B.* **72** (2017) 17-30.
105. Zeng Y., Lu C., Rong C., Tao X., Liu X., Liu R., Liu M. - Analysis and design of asymmetric mid-range wireless power transfer system with metamaterials, *Energies.* **14** (2021) 1-10. <https://doi.org/10.3390/en14051348>.
106. Brizi D., Fontana N., Barmada S., Monorchio A. - An accurate equivalent circuit model of metasurface-based wireless power transfer systems, *IEEE Open J. Antennas Propag.* **1** (2020) 549-559. <https://doi.org/10.1109/OJAP.2020.3028297>.
107. Brizi D., Stang J. P., Monorchio A., Lazzi G. - A compact magnetically dispersive surface for low-frequency wireless power transfer applications, *IEEE Trans. Antennas Propag.* **68** (2020) 1887-1895. <https://doi.org/10.1109/TAP.2020.2967320>.
108. Correa D. C., Resende U. C., Bicalho F. S. - Experiments with a compact wireless power transfer system using strongly coupled magnetic resonance and metamaterials, *IEEE Trans. Magn.* **55** (2019) 8401904. <https://doi.org/10.1109/TMAG.2019.2913767>.
109. Pham T. S., Khuyen B. X., Tung B. S., Hoang T. T., Pham V. D., Ngo Q. M., Lam V. D. - Enhanced efficiency of asymmetric wireless power transmission using defects in 2D magnetic metamaterials, *J. Electron. Mater.* **50** (2021) 443-449. <https://doi.org/10.1007/s11664-020-08586-w>.
110. Duong T. P., Lee J. W. - A dynamically adaptable impedance-matching system for midrange wireless power transfer with misalignment, *Energies.* **2015** (2015) 7593-7617.

- <https://doi.org/10.3390/en8087593>.
111. Ranaweera A. L. A. K., Moscoso C. A., Lee J. W. - Anisotropic metamaterial for efficiency enhancement of mid-range wireless power transfer under coil misalignment, *J. Phys. D. Appl. Phys.* **48** (2015) 1-8. <https://doi.org/10.1088/0022-3727/48/45/455104>.
 112. Wang S., Jiang C., Tao X., Chen F., Rong C., Lu C., Zeng Y., Liu X., Liu R., Wei B., Liu M. - Enhancing the stability of medium range and misalignment wireless power transfer system by negative magnetic metamaterials, *Materials (Basel)*. **13** (2020) 1-11. <https://doi.org/10.3390/ma13245695>.
 113. Lee W., Yoon Y. K. - Tunable metamaterial slab for efficiency improvement in misaligned wireless power transfer, *IEEE Microw. Wirel. Components Lett.* **30** (2020) 912-915. <https://doi.org/10.1109/LMWC.2020.3015680>.
 114. Kim J., Kim J., Kong S., Kim H., Suh I. S., Suh N. P., Cho D. H., Kim J., Ahn S. - Coil design and shielding methods for a magnetic resonant wireless power transfer system, *Proc. IEEE*. **101** (2013) 1332-1342. <https://doi.org/10.1109/JPROC.2013.2247551>.
 115. Lipworth G., Ensworth J., Seetharam K., Lee J. S., Schmalenberg P., Nomura T., Reynolds M. S., Smith D. R., Urzhumov Y. - Quasi-Static Magnetic Field Shielding Using Longitudinal Mu-Near-Zero Metamaterials, *Sci. Rep.* **5** (2015) 1-8. <https://doi.org/10.1038/srep12764>.
 116. Lu C., Huang X., Rong C., Hu Z., Chen J., Tao X., Wang S., Wei B., Liu M. - Shielding the magnetic field of wireless power transfer system using zero-permeability metamaterial, *J. Eng.* **2019** (2019) 1812-1815. <https://digital-library.theiet.org/content/journals/10.1049/joe.2018.8678>.
 117. Markvart A., Song M., Glybovski S., Belov P., Simovski C., Kapitanova P. - Metasurface for near-field wireless power transfer with reduced electric field leakage, *IEEE Access*. **8** (2020) 40224-40231. <https://doi.org/10.1109/ACCESS.2020.2976755>.
 118. Pham T. S., Ranaweera A. K., Lam V. D., Lee J. W. - Experiments on localized wireless power transmission using a magneto-inductive wave two-dimensional metamaterial cavity, *Appl. Phys. Express*. **9** (2016) 1-4. <https://doi.org/10.7567/APEX.9.044101>.
 119. Bui H. N., Pham T. S., Ngo V., Lee J. W. - Investigation of various cavity configurations for metamaterial-enhanced field-localizing wireless power transfer, *J. Appl. Phys.* **122** (2017) 1-10. <https://doi.org/10.1063/1.5001130>.
 120. Bui H. N., Pham T. S., Kim J. S., Lee J. W. - Field-focused reconfigurable magnetic metamaterial for wireless power transfer and propulsion of an untethered microrobot, *J. Magn. Magn. Mater.* **494** (2020) 1-13. <https://doi.org/10.1016/j.jmmm.2019.165778>.
 121. Bui H. N., Pham T. S., Lee J. W. - Active switching control of field-localized waveguide using time-modulated non-reciprocal reconfigurable metasurface, *Results Phys.* **27** (2021) 1-9. <https://doi.org/10.1016/j.rinp.2021.104467>.
 122. Pham T. S., Ranaweera A. K., Ngo D. V., Lee J. W. - Analysis and experiments on Fano interference using a 2D metamaterial cavity for field localized wireless power transfer, *J. Phys. D. Appl. Phys.* **50** (2017) 1-10. <https://doi.org/10.1088/1361-6463/aa7988>.
 123. Ranaweera A. L. A. K., Pham T. S., Bui H. N., Ngo V., Lee J. W. - An active metasurface for field-localizing wireless power transfer using dynamically reconfigurable cavities, *Sci. Rep.* **9** (2019) 1-12. <https://doi.org/10.1038/s41598-019-48253-7>.